Oil & Gas Science and Technology – Rev. IFP Energies nouvelles **75**, 51 (2020)

https://doi.org/10.2516/ogst/2020038

Available online at:
ogst.ifpenergiesnouvelles.fr

REGULAR ARTICLE OPEN ACCESS

Geological sequestration of CO_2 in a water-bearing reservoir in hydrate-forming conditions

Raghvendra Pratap Singh, Karanpal Singh Shekhawat, Malay K. Das*, and Krishnamurthy Muralidhar

Department of Mechanical Engineering, Indian Institute of Technology Kanpur, 208016 Kanpur, India

Received: 31 December 2019 / Accepted: 25 May 2020

Abstract. Higher concentration of carbon dioxide in the atmospheric air is a major environmental challenge and requires immediate attention for quicker mitigation. In that respect, the novel idea of CO_2 sequestration in geological settings is worth examining from a quantitative perspective. In the present study, numerical simulation of CO_2 injection into a porous reservoir is performed. The selected reservoir presents suitable thermodynamic conditions for CO_2 hydrate formation. Unsteady simulations are carried out in one space dimension under isothermal and non-isothermal frameworks. An additional simulation of CO_2 injection in a depleted methane hydrate reservoir is also reported. In the present study, the response of the reservoir to storage of CO_2 is analyzed with respect to four parameters – reservoir porosity, initial water saturation and reservoir temperature and injection pressure. Quantities of interest are hydrate formation patterns and the cumulative CO_2 mass sequestration in the reservoir as a function of time. Numerical experiments show that the initial water saturation is an important parameter as it affects both CO_2 gas migration and hydrate formation. Isothermal simulation yields results that are similar to the non-isothermal model, thus suggesting that the isothermal assumption may be adopted for future CO_2 injection studies. Hydrate formation rate of CO_2 near the injection well is found to be one order of magnitude higher than the interior but its magnitude is quite small when compared to water and gas saturations. Higher injection pressure leads to a continuous increase in injected mass of CO_2 primarily due to increased gas density, though an increase in hydrate formation near the injection well is also observed. Lower reservoir temperature supports a higher amount of hydrate formation from the injected mass of CO_2 and is clearly desirable.

Nomenclature

A_{cs}	Cross-sectional area of reservoir (m^2)
A_{SH}	Specific area of hydrates (m^2)
C_p	Specific heat capacity (J/kg K)
ΔE	Activation energy (J)
H	Enthalpy (J/kg)
ΔH_h^f	Enthalpy of hydrate formation (J/kg)
K_{abs}	Absolute permeability (m^2)
K_f	Hydrate formation rate [mol/Pa s m^2]
$k_{r\gamma}$	Relative permeability for phase
L	Reservoir length (m)
λ_{eff}	Equivalent thermal conductivity (W/m K)
M^i	Molar mass of specie i (kg/mol)
$M_g^{CO_2}$	Mass of CO_2 in gas form (kg)
M_g^{init}	Initial mass of CO_2 gas in reservoir (kg)
N_h	Hydration number
P	Pressure (MPa)
P_{cs}	Perimeter of cross-section (m)
P_{eq}	Equilibrium pressure of CO_2 hydrate
R	Universal gas constant (kg/kmol K)
S_γ	Saturation of phase γ
T	Temperature (K)
t	Time (s)
U	Internal energy (J/kg)
x	Horizontal coordinate axis (m)

Greek symbols

α	Coefficient-of-heat-transfer (W/m^2 K)
γ	Phase
λ	Thermal conductivity (W/m K)
μ	Viscosity
ρ	Density
ϕ	Porosity
ω	Mass fraction

Superscripts and subscripts

c	Carbon dioxide
g	Gas phase

* Corresponding author: mkdas@iitk.ac.in

h	Hydrate phase
l	Liquid phase
s	Solid matrix
w	Water component

1 Introduction

It is now an established fact that unrestrained emission of Carbon dioxide (CO_2) into atmospheric air is adversely affecting the earth's ecosystem [1, 2]. In this context short to medium term solution of safe CO_2 disposal should be examined. Geological storage of carbon dioxide is considered one of most viable option for CO_2 disposal [3, 4] as it is estimated that several geological sites have the potential to store millions of tons of CO_2 by various physical and chemical mechanisms [5]. Deep ocean floor provides ideal vast geological space for CO_2 storage in liquid and hydrate state [6–8]. However, probable CO_2 leakage and adverse impact on local ecology prohibit large scale CO_2 injection. Depleted oil and gas fields present themselves as most suitable storage site though their storage capacity is very limited [9]. Sequestration of CO_2 as hydrate, in thermodynamically suitable geological sediments is a promising idea [10–12] and justifies in-depth investigation of storage capacity with respect to geological parameters, injection conditions, and initial reservoir conditions. The idea of CO_2 sequestration in hydrate form becomes more relevant as vast deposits of natural gas-hydrate deposits are expected to be exploited in the future, leaving large vacant space available for CO_2 storage. These reservoirs not only provide suitable thermodynamic conditions for CO_2 hydrate formation but also cover a huge geological volume, making them relevant for expected rates of CO_2 disposal.

Gas hydrates are a solid crystalline compound, formed at high pressure and low temperature thermodynamic conditions [13]. Pure CO_2 forms *s*I type structures which is identical to the pure CH_4 structure. Theoretically each unit volume of CO_2 hydrate contains ~170 units of CO_2 gas at STP in the case of 100% cage occupancy [13–16]. Apart from storing the gas under compressed conditions, this approach represents a second opportunity to store CO_2 in concentrated form with a diminished possibility of leakage. The appearance of a large quantity of hydrate in the reservoir requires detailed analysis with regard to operational, geological and thermodynamic conditions within the reservoir. There are certain sub-seabed shallow aquifers (<300 m from sea surface), located in colder oceanic sub surfaces of Japan sea, Northern Pacific Ocean, Northern Atlantic Ocean, Arctic ocean, and the Antarctic ocean [8, 17] where temperature conditions of <5 °C are realized. These are suitable for hydrate formation and permit storage of CO_2 as hydrates. This chemical route of storage is an advantage because of the leakage possibility of CO_2 stored in gaseous form. A second advantage indicated by various authors is that the injected CO_2, few meters below the subsurface, will rise and block the probable leakage paths by forming CO_2 hydrates in the solid phase.

Negative Buoyancy Zone (NBZ) is defined as the depth below the seabed where liquid CO_2 density is higher than resident seawater density. The Hydrate Formation Zone (HFZ) is the thickness of seabed where thermodynamic conditions are within the CO_2 hydrate stability zone. Fate of the injected liquid CO_2 beneath the deep seabed sediments below the NBZ and the HFZ was studied by Qanbari *et al.* [18, 19]. The authors concluded that liquid CO_2 can be effectively trapped beneath NBZ and HFZ for considerably longer period of time because of dual trapping mechanisms of gravitational stability and hydrate formation.

The CO_2 storage capacity of a porous medium and *in situ* hydrate formation kinetics are directly affected by the reservoir properties such as porosity and permeability. Several laboratory experiments have been conducted primarily to observe and quantify the process. CO_2 hydrate formation during liquid-CO_2 injection in packed bed mimicking seabed was studied by Abe *et al.* [20]. The authors analysed liquid-CO_2 two phase flow in hydrate forming and non-hydrate forming conditions and reported strong influence of heat dissipation on hydrate formation. Investigation of CO_2 hydrate formation was carried out experimentally by Zhou *et al.* [21] in a high pressure flow loop. The authors examined several important parameters for hydrate formation and its morphological evolution. Hydrate morphology is important as the reactive surface area correlates to it. The authors also analysed induction time for CO_2 hydrate formation. Recently, CO_2 sequestration in the form of hydrates in a laboratory setup mimicking depleted methane hydrate reservoir was evaluated by Liu *et al.* [22] using magnetic resonance imaging. The study also investigated the effect of combined CO_2–water injection on CO_2-hydrate formation. It was found that a relatively slow injection rate of the mixture gives better response in terms of the amount of hydrate formed. Zhang *et al.* [23] recently studied the effect of interlayered geological system on CO_2 storage with the objective to help in selection of suitable storage site.

Numerical simulations of gaseous CO_2 injection into a depleted gas field mimicking conditions similar to Northern Alberta, Canada were carried out by Zatsepina and Pooladi-Darvish [24]. One of the important observations of the study was higher hydrate saturation near the lower and upper bounding rocks primarily due to quick dissipation of heat. It signifies the important role of confining media and its role in absorbing heat due to hydrate formation. At the same time, the authors also found that CO_2 injection at a controlled temperature avoids hydrate formation near the well bore. Truthful estimation of reservoir potential, its response to injected CO_2 and hydrate formation dynamics are important aspects which require field experiments. Ignik Sikumi field test was conducted with the aim of testing the feasibility of CO_2–CH_4 exchange process for methane recovery from hydrate reservoirs [25]. The field trial confirmed the possibility CO_2 injection for natural gas production with 60% of injected CO_2 sequestered in various forms. However, field scale trials are expensive and can only be performed for a limited time period. In this respect, numerical simulation provides a convenient alternative.

The literature survey presented above confirms the possibility of CO_2 sequestration as hydrate in geological formation having suitable thermodynamic conditions for hydrate formation. It was pointed out that there are several influencing parameters including porosity, permeability, water content, and temperature. However, most of the studies in the literature are limited to laboratory scale experiments and have addressed estimation of hydrate kinetics, studying the feasibility CO_2–CH_4 replacement and quantification of the effect of pore size on water to hydrate conversion. There are limited studies related to field-scale experiments, either numerically or experimentally, with the exception of the Ignik Sikumi field test. Thus, there is a knowledge gap arising out of CO_2 disposal on a field scale over a long period of time. As a substitute for field-scale experiments, numerical studies are a viable option to narrow the knowledge gap. The present study considers injection of gaseous CO_2 in a geological reservoir and its storage in the form of hydrates. The numerical framework is based on one dimensional mass, momentum, and energy transport with detailed modeling of chemical kinetics and thermodynamics of phase equilibrium. The geological reservoir is taken to be spread over a horizontal dimension and its thickness in the vertical direction is taken to be small, so that a one dimensional approximation is applicable. This approach provides a computationally efficient framework for examining the sensitivity of the sequestration process to parameters such as injection pressure, reservoir temperature, porosity, and water saturation.

The major objectives of the present work are as follows:

1. Examine the effect of initial water saturation on CO_2 transport and hydrate formation.
2. Study near-injection well dynamics of hydrate formation and possibility of well blockage.
3. Study effect of changes in porosity and initial reservoir temperature on storage capacity.
4. Compare isothermal and non-isothermal modeling approaches for CO_2-hydrate sequestration.
5. Explore CO_2 sequestration in a depleted methane hydrate reservoir in terms of storage capacity and its comparison with methane-free reservoirs.

The ensuing sections describe the mathematical model and solution methodology, followed by results and conclusions drawn.

2 Mathematical model

Physical processes involved in CO_2 sequestration in a hydrate reservoir are complex as they involve phenomena differing substantially from one another in terms of length and timescales. Some of these take place within the pore space at the liquid–gas interface including dissolution – degasification of CO_2 from water, and evaporation–condensation of water. These processes occur at small length scales but are rapid, generating small timescales. Hydrate formation, which takes place at the hydrate–gas or hydrate–water interface, also takes place within pore volume but is slower than these two processes. The effect of the curvature of the gas–water interface on the momentum equation is captured via the treatment of capillary pressure. Processes that occur at the reservoir scale are migration of the fluid phases in porous media and thermal energy transport through advection and diffusion. Those occurring at the reservoir scale have longer timescale as compared to the pore scale except for the hydrate formation reaction. From a modeling perspective, it is difficult to include all the complexities arising from a hierarchy of length and timescales since it can result in excessive computational effort. In the present study, short timescale phenomena are treated as instantaneous and small length scales arising from liquid to gas interface are phenomenologically modeled. The simplified approach to modeling that is appropriate for long term injection of CO_2 in a field scale reservoir is presented below.

In the present work, a transient, non-isothermal, multiphase model for simulation of CO_2 injection and sequestration in a hydrate bearing porous media is considered. The mathematical model accounts for three phases – gaseous, aqueous, and CO_2-hydrate; and three components, namely, water, CO_2, and CO_2-hydrate. The first two phases, water and CO_2, are mobile while the hydrate phase is immobile. The three phases are considered to be in local thermal equilibrium with each other along with the solid matrix of the porous media. The solubility of CO_2 gas in aqueous phase and presence of water vapour in gas phase can be readily accounted for in the model but are not discussed. The modeled governing equations and constitutive relations are presented in the following sections.

2.1 Governing equations

One-unit mole of CO_2 combines with N_h moles of H_2O to form one mole of CO_2-hydrate as given by equation (1) [26]:

$$CO_2 + N_h H_2O \Longleftrightarrow CO_2 \cdot N_h H_2O, \tag{1}$$

here, N_h is the hydration number which defines the number of H_2O molecules attached to one molecule of CO_2. In non-isothermal, multiphase, and multi-component systems, it is easier to deal with mass balance formulation for the components rather than phase balance. Equations (2)–(4) adapted from Sun *et al.* [26] are mass balance equations for CO_2-hydrate, water, and CO_2 mass components with source terms arising from the hydrate reaction, equation (1):

$$\frac{\partial(\phi\rho_h S_h)}{\partial t} = \dot{m}_h, \tag{2}$$

$$\frac{\partial(\phi\rho_l S_l)}{\partial t} + \frac{\partial}{\partial x}(\rho_l V_l) = \dot{m}_l, \tag{3}$$

$$\frac{\partial(\phi\rho_g S_g)}{\partial t} + \frac{\partial}{\partial x}(\rho_g V_g) = \dot{m}_g. \tag{4}$$

The quantity $\dot{m}_h$ in equation (2) represents the local mass rate of hydrate formation per unit volume in a hydrate formation reaction given by equation (1). The quantities

$\dot{m}_l$ and $\dot{m}_g$ in equations (3)–(4) represent the local mass rate of water and gas produced per unit volume, respectively.

As in porous media flows, the pore velocity is taken to be small ($\mathrm{Re}_{dp} << 1$ where subscript dp is pore diameter) so that the flow is viscous dominated and the creeping flow hypothesis is valid. In this situation, Darcy's law is valid though theoretically it is possible to derive it from the Navier–Stokes equations. Darcy's law in an unsaturated medium for phase γ is given by equation (5) [26]:

$$V_\gamma = -\frac{K_{\mathrm{abs}} k_{r\gamma}}{\mu_\gamma} \frac{\partial}{\partial x} P_\gamma, \tag{5}$$

here, V_γ, $k_{r\gamma}$, μ_γ, P_γ, ρ_γ are velocity, relative permeability, dynamic viscosity, pressure, and density for phase γ respectively. Effect of phase interface on fluid mobility is captured by the relative permeability function $k_{r\gamma}$. When local energy exchange phenomena at the pore scale are much faster than over the reservoir scale, local thermal equilibrium is a valid approximation and a single energy equation is sufficient to determine energy transport. The energy equation in terms of a local phase-averaged temperature is given by equation (6) [26, 27]:

$$\frac{\partial}{\partial t}\left(\phi \sum_\gamma \rho_\gamma S_\gamma U_\gamma + (1-\phi)\rho_s U_s\right) + \sum_{\gamma=\mathrm{l,g}} \left(\sum_{i=\mathrm{c,w}} \nabla \cdot \rho_\gamma V_\gamma \omega_\gamma^i H_\gamma^i \right)_{\mathrm{w}} = \nabla \cdot (\lambda_{\mathrm{eff}} \nabla T) + \dot{m}_h \Delta H_h^f + \dot{E}. \tag{6}$$

The phenomenon of the Joule–Thomson coefficient and the resulting temperature reduction are important when the expansion of CO_2 takes place in free space. However, its effect on REV-averaged temperature changes is small when the expansion takes place in porous media at moderate pressure gradients [28, 29]. An order of magnitude analysis carried out by the authors showed the maximum temperature reduction to be 0.03 K near the injection well for short time, and negligible elsewhere. Hence, the present study excludes the Joule–Thomson effect in the thermal energy equation.

Thus, physical transport process of CO_2 injection in porous media initially filled with gaseous CO_2 and water is governed by four partial differential equations arising out of mass and energy balances. Hydrate reaction equation (Eq. (4)) is assumed to be slower than other pore scale processes. The four governing equations contain several parameters that are required *a priori* to be specified. In addition, initial and boundary conditions needed to close the above mathematical formulation are discussed below.

2.2 Constitutive relationships

Transport models developed for transfer of mass (including species), momentum, and thermal energy depend upon several parameters and their dependence on system variables needs to be established. System variables are quantities needed to completely define the state of the multiphase porous medium. These include relations connecting phase pressures and saturations, temperature, and mass fractions. Quantities calculated by solving the governing equations are primary variables whereas those which are estimated from primary variables are termed secondary. Hydrodynamic and thermal parameters, necessary to close the governing equations are estimated from state variables through empirical correlations.

For the present work, CO_2 in the gas phase is taken to behave as an ideal gas and given by equation (7). Mass fractions of H_2O and CO_2 in hydrate phase depend upon hydration number and molecular masses of H_2O and CO_2 and can be evaluated using the following stoichiometric relationship given in equations (8) and (9) [30] below:

$$P_g = \rho_g \frac{R_u}{M_g} T, \tag{7}$$

$$\omega_h^{CO_2} = \frac{M^{CO_2}}{M^{CO_2} + N_h M^w}, \tag{8}$$

$$\omega_h^{w} = \frac{N_h M^w}{M^{CO_2} + N_h M^w}. \tag{9}$$

In the original model of Kim *et al.* [31], formation kinetics is driven by the difference in fugacities of gas and hydrate components. A modified Kim–Bishnoi type of kinetic model is assumed for the reaction process which is governed by equation (10) [31]. According to this model, the hydrate formation rate is directly proportional to a driving force which is defined by the difference between the CO_2 pressure in gas phase and hydrate equilibrium pressure and this relationship is described as:

$$[\dot{m}_h]_f = M_h^{CO_2}\left(\phi A_{SH} S_l + \phi^2 A_{SH} S_l S_h\right) K_f^{CO_2} \times \exp\left(-\frac{\Delta E^{CO_2}}{RT}\right)\left(P_g^{CO_2} - P_{eq}^{CO_2}\right). \tag{10}$$

Hydrate formation consumes resident water and CO_2 and their rates are evaluated with the help of formation rate of hydrate and stoichiometric relationship as given by equation (11) [26, 30]:

$$\dot{m}_g = -\dot{m}_h\left(\frac{M^{CO_2}}{M^h}\right), \quad \dot{m}_w = -\dot{m}_h\left(\frac{N_h M^w}{M^h}\right). \tag{11}$$

Figure 1 presents the three phase equilibrium curves of CO_2-hydrate, CH_4-hydrate and pure CO_2. Phase curve for CO_2 hydrate is given by equation (12) and correlation for CH_4-hydrate is adapted from Adisasmito *et al.* [32]. The vapour pressure equation of CO_2 as a function of temperature is used to determine its state on the phase diagram. In the present mathematical model, CO_2 mass is assumed to be present in the gaseous phase alone, while CO_2 hydrate is in the solid immobile phase. The vapour pressure of CO_2 from the triple point temperature up to the critical temperature is given by equation (13) [33]:

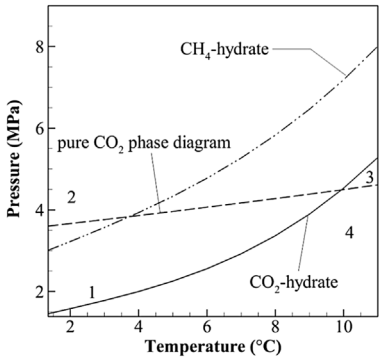

Fig. 1. CO_2 and CH_4 hydrate phase equilibrium curves along with pure CO_2 phase diagram. CO_2 hydrate curves and CO_2 phase diagram divide the region into four zones 1–4. Zones 1 and 2 are within stable hydrate conditions and zones 3 and 4 are outside of stable conditions. Zone 1 is of interest in the present work.

$$P_{\text{eq}}^{\text{CO}_2} = \left[0.06539\left(\frac{T-278.9}{3.057}\right)^3\right] + \left[0.2738\left(\frac{T-278.9}{3.057}\right)^2\right] + \left[0.9697\left(\frac{T-278.9}{3.057}\right)\right] + 2.479, \tag{12}$$

$$\ln\left(\frac{P_{\text{sat}}}{P_{\text{c}}}\right) = \frac{T_{\text{c}}}{T}\left[\sum_{i=1,4} a_i\left(1-\frac{T}{T_{\text{c}}}\right)^{t_i}\right]. \tag{13}$$

The presence of a solid hydrate directly affects the effective permeability as it progressively fills the pore space and reduces the effective porosity. The expression for effective porosity, ϕ_{lg}, defined as the actual pore volume available to mobile phases is given by equation (14) below. In the present formulation, absolute permeability of the medium is modeled as a function of the effective fluid porosity, equation (15) [26]. These expressions are given as follows:

$$\phi_{\text{lg}} = (1 - S_{\text{h}})\phi, \tag{14}$$

$$K_{\text{abs}} = 5.51721\left(\phi_{\text{lg}}\right)^{0.86} \times 10^{-15}\ \text{m}^2. \tag{15}$$

Permeability impairment caused by hydrate blockage of the pore space is only approximately described by equations (14) and (15). However, present work is a baseline study on CO_2 sequestration and the impairment model is chosen from the literature on methane recovery from gas hydrate reservoirs. There are other impairment models reported [34] for halite precipitation. However, this cannot be generalized to CO_2 hydrates since the physical mechanism of halite precipitation in the pore space is non-uniform and distinct from hydrate formation, which in turn may occur at the phase boundary.

Relative permeability measures the flow obstruction created by other mobile phases separated by an interface present in the pore volume. In case of two mobile phases (water and gas), two equations exist for each phase and the same are given by equation (16) [26] for water and gas phases respectively. There, parameters n_{l} and n_{g} represent the pore size distribution of porous media while parameters S_{lr} and S_{gr} represent the irreducible quantity of each phase. Similarly, capillary pressure function which is a measure of averaged interface curvature between two mobile phases in any given elementary volume is given by equation (17) [26]. These expressions are given below:

$$k_{\text{rl}} = \left[\frac{\frac{S_{\text{l}}}{S_{\text{l}}+S_{\text{g}}} - S_{\text{lr}}}{(1 - S_{\text{lr}} - S_{\text{gr}})}\right]^{n_{\text{l}}}, \quad k_{\text{rg}} = \left[\frac{\frac{S_{\text{g}}}{S_{\text{l}}+S_{\text{g}}} - S_{\text{gr}}}{(1 - S_{\text{lr}} - S_{\text{gr}})}\right]^{n_{\text{g}}}, \tag{16}$$

$$P_{\text{c}} = P_{\text{ec}}\left[\frac{\frac{S_{\text{l}}}{S_{\text{l}}+S_{\text{g}}} - S_{\text{lr}}}{(1 - S_{\text{lr}} - S_{\text{gr}})}\right]^{-n_{\text{c}}}. \tag{17}$$

Saturations of all phases add up to unity and the sum of all phase volumes present in pore space is equal to the total pore volume. This constraint is expressed as:

$$S_{\text{g}} + S_{\text{l}} + S_{\text{h}} = 1. \tag{18}$$

Specific heat capacities for CO_2 gas and water at constant pressure are taken as a function of temperature and given as equations (19) and (20) [26, 30].

$$C_{\text{pg}}^{\text{CO}_2} = 505.11 + (1.1411\,T) - \left(89.139 \times 10^{-5}\,T^2\right) + \left(210.566 \times 10^{-9}\,T^3\right) \quad \text{J/kg K}, \tag{19}$$

$$C_{\text{pl}}^{\text{w}} = 4023.976 + (0.57736\,T) - \left(8.314 \times 10^{-5}\,T^2\right) \quad \text{J/kg K}. \tag{20}$$

The enthalpy of CO_2-hydrate formation is given by equation (21) [30, 35]:

$$\Delta H_{\text{h}}^{\text{f}} = \left(2528\left(\frac{T-278.15}{2.739}\right)^8\right) + \left(75.36\left(\frac{T-278.15}{2.739}\right)^7\right) - \left(9727\left(\frac{T-278.15}{2.739}\right)^6\right) + \left(1125\left(\frac{T-278.15}{2.739}\right)^5\right) + \left(4000\left(\frac{T-278.15}{2.739}\right)^4\right) - \left(4154\left(\frac{T-278.15}{2.739}\right)^3\right) + \left(14,430\left(\frac{T-278.15}{2.739}\right)^2\right) - \left(6668\left(\frac{T-278.15}{2.739}\right)\right) + 389,900 \quad \text{J/kg K}. \tag{21}$$

The lateral heat transfer to the bounding impermeable rocks is given a symbol E. Let P_{cs} and A_{cs} be the perimeter and cross-sectional area of the reservoir and α, the coefficient-of-heat-transfer between the hydrate layer and bounding rocks. Then, the heat gain from the surrounding per unit volume is obtained as Sun *et al.* [26]:

$$E = \frac{P_{\text{cs}}}{A_{\text{cs}}}\alpha(T_{\text{init}} - T). \tag{22}$$

As the porous media contains several phases in a given elementary volume, the equivalent thermal conductivity in the analysis is calculated assuming layers of phases arranged in series inside porous media. Let λ_γ be the thermal conductivity of phase γ; then, the equivalent conductivity is given as equation (23) [30]:

$$\frac{1}{\lambda_{\text{eff}}} = \frac{\phi S_{\text{l}}}{\lambda_{\text{l}}} + \frac{\phi S_{\text{g}}}{\lambda_{\text{g}}} + \frac{\phi S_{\text{h}}}{\lambda_{\text{h}}} + \frac{(1-\phi)}{\lambda_{\text{s}}}. \tag{23}$$

CO_2 gas injection rate at the injection well is obtained by velocity estimated by Darcy's law and is written as equation (24) below. The total mass of CO_2 gas injected is calculated by integrating the equation (24) with respect to time. The CO_2 gas injection rate is given as follows:

$$\dot{M}_{\text{g}}^{\text{inj}} = \rho_{\text{g}} A_{\text{cs}} \left(-\frac{K k_{\text{rg}}}{\mu_{\text{g}}} \frac{\partial P_{\text{g}}}{\partial x} \right)\Bigg|_{x=0}. \tag{24}$$

The total mass of CO_2 initially present in the gas phase in the reservoir is calculated as:

$$M_{\text{g}}^{\text{init}} = L A_{\text{cs}} \phi S_{\text{g}} \left(-\frac{P_{\text{g}} M^{\text{CO}_2}}{RT} \right). \tag{25}$$

The total amount of CO_2 that should be present in the reservoir either in the form of hydrate or gas at any time must be equal to addition of the injected and initial mass of CO_2 gas. At any time, mass of CO_2 in hydrate and gas form is calculated by spatial integration given below:

$$M_{\text{h}}^{\text{CO}_2} = \int_0^L A_{\text{cs}} \phi S_{\text{h}}(x) \rho_{\text{h}} \left(\frac{M^{\text{CO}_2}}{M^{\text{CO}_2} + N_{\text{h}} M^{\text{w}}} \right) \text{d}x, \tag{26}$$

$$M_{\text{g}}^{\text{CO}_2} = \int_0^L A_{\text{cs}} \phi S_{\text{g}}(x) \left(\frac{P_{\text{g}}(x) M^{\text{CO}_2}}{RT(x)} \right) \text{d}x. \tag{27}$$

The above set of governing equations and parameters are applicable when CO_2 is injected in reservoir which is initially filled with CO_2 gas and water. The important parameters and constants that are used to solve the above set of equations are adapted from [30, 36, 37] and summarized in Table 1. The present study considers higher water saturation in a depleted hydrate reservoir to be an appropriate initial condition. Also, a prospective site for CO_2-hydrate sequestration should have sufficient *in-situ* water for hydrate formation.

The set of governing equations applicable for the test case when CO_2 is injected in a depleted CH_4-hydrate reservoir is discussed by Khetan *et al.* [30]. This formulation with appropriate change in process parameters and boundary conditions has been utilized in the present work. Furthermore, a more detailed and comprehensive presentation of the mathematical model can be found elsewhere [24, 26, 27, 36–39].

2.3 Physical domain, initial, and boundary conditions

A schematic drawing of the physical reservoir considered for a study of CO_2 sequestration is shown in Figure 2. It is a geological sediment, 10 m thick, spread horizontally and is bounded by an impermeable layer above and below. The numerical study is conducted on 500 m length of the reservoir. Since the thickness is small compared to the length, a one-dimensional model has been adopted for analysis. Exchanges of energy with the upper and lower impermeable layers are modeled as energy sink terms in the one-dimensional framework. The left-hand side of the domain ($x = 0$) is the injection well and right most end ($x = 500$ m) is insulated. A total of 17 simulations are conducted on the prescribed geometry for varying porosities, initial water saturations, initial reservoir temperature, and injection pressure. The simulation parameters for the test cases are summarized in Table 2. Test cases 1–9 are studies in a non-isothermal framework; test cases 10–16 are isothermal studies for reservoirs initially filled with CO_2 gas and water. Test case 17 is a study of CO_2 injection in a depleted hydrate reservoir which initially contains CH_4 gas and water. Initial thermodynamic conditions are similar in all cases.

The reservoir is partially saturated with water and CO_2 gas (cases 1–16) at thermodynamic conditions that lie within the unstable hydrate zone but close to the CO_2-hydrate phase equilibrium curve. During operation, CO_2 gas is introduced at the injection well with pressure greater than the reservoir. It is below the saturation pressure so as to avoid the formation of liquid CO_2. For a temperature of 279 K, CO_2 liquefies when pressure is increased beyond 4 MPa. Thus, an injection pressure above 4 MPa and a temperature below 279 K are not used in the simulation as the present model is restricted to CO_2 present either in the gas phase or as a solid hydrate. Also, it is assumed that no ice formation takes place within the reservoir. It necessitates that temperature is everywhere above the quadruple point of the hydrate, gas, water and ice, namely, 273.15 K. The vapour pressure equation of CO_2, equation (13), as a function of temperature is used to check that the state of CO_2 is in gas or liquid phase at all times during the injection operation.

3 Numerical methodology

A second order finite difference method is used for the discretization of the differential governing equations. Discretization of the governing equations results in Tri-Diagonal coefficient Matrices which are inverted using the Thomas (TDMA) Algorithm. Euler time stepping is used to march the solution in time. Within each time step, the governing equations are solved sequentially in an implicit manner. Within each time step, governing equations are solved iteratively till a converged solution is obtained. It is noted that the equations are not only nonlinear but coupled as well, necessitating an iterative solution. The initial guess of the solution variables at the new time step is taken to be the values acquired at the previous time level. The sequence of calculations can affect convergence. In this respect, for each iteration loop for the solution of the governing equations, mass conservation equation, equation (2), is solved first for the hydrate saturation, S_{h}. It should be noted that equation (2) is an ODE as hydrate phase is immobile and requires only an initial condition. The aqueous phase saturation, S_{l}, is solved next using the mass conservation

Table 1. Parameters and their numerical values used in base case simulation.

Physical meaning	Value
Hydration number (N_h)	6
Porosity (ϕ)	0.28
Initial temperature of reservoir (T_{init})	279 K
Initial gas pressure in reservoir (P_{init})	2.51 MPa
Initial water saturation (S_{w0})	0.9
Initial hydrate saturation (S_{h0})	0
Initial gas saturation (S_{g0})	0.1
Aqueous phase density (ρ_l)	1000 kg/m^3
Solid rock phase density (ρ_s)	2675.1 kg/m^3
CO_2 hydrate phase density (ρ_h)	1100 kg/m3
CO_2 hydrate heat capacity (C_p^h)	2220 J/kg K
Perimeter of the cross-section (Pcs)	22 m
Area of the cross-section (Acs)	10 m^2
Hydrate formation rate constant (K_f)	0.35 m mol/Pa s m^2
Specific area of hydrates (A_{SH})	375 000 m^2/m^3
Activation energy for CO_2 hydrate (ΔE)	81 084 J/mol
Aqueous phase viscosity (μ_l)	1 mPa s
Viscosity of CO_2 in gas phase (μ_g^c)	1.48 × 10^{-5} Pa s
Entry capillary pressure (P_{ec})	5000.0 Pa
Constant for capillary pressure (n_c)	0.65
Irreducible gas phase saturation (S_{gr})	0.0
Irreducible aqueous phase saturation (S_{lr})	0.2
Relative permeability constant for liquid (n_l)	4
Relative permeability constant for gas (n_g)	2
CO_2 hydrate heat capacity (C_p^h)	2220 J/kg-K
CO_2 gas injection pressure (P_{inj})	4 MPa
CO_2 gas injection temperature (T_{inj})	279 K

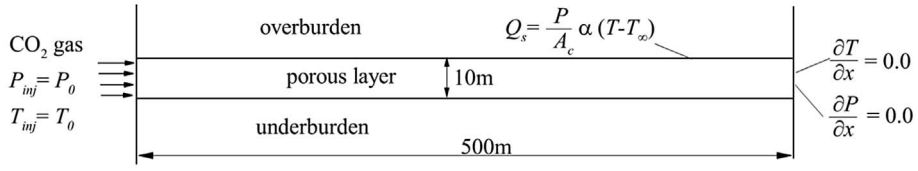

Fig. 2. Schematic drawing of the hydrate reservoir considered in the present simulation along with the boundary conditions enforced. Related parameters and properties are given in Table 1.

equation of water component, equation (3). Saturation of gas phase is calculated by the saturation constraint given by equation (18). After calculation of the phase saturations, gas phase pressure is calculated from equation (4) which is a mass conservation equation for the CO_2 component. For gas pressure, P_g, as a dependent variable, equation (4) behaves like a parabolic equation and is convenient to solve using Thomas Algorithm (TDMA). The aqueous phase pressure is obtained with the help of equation (17) which is a relation between gas and aqueous phase pressure connected through the capillary pressure. Capillary pressure, P_c, is a function of aqueous phase saturation which is known at this stage. Reservoir temperature, T, is finally calculated from the energy equation, equation (6). After an update of a time step of the governing equations, parameters and secondary variables are updated and convergence is examined. After convergence, the solver proceeds to the new time step.

3.1 Validation

The solution algorithm and the computer code of the present study have been extensively validated against the previous literature wherein the authors have numerically simulated two-phase flow and depressurization induced gas recovery both from a 1D laboratory core sample and

Table 2. Test cases of simulation considered for the present work.

Test cases	Reservoir porosity	Initial water saturation	Initial reservoir temperature (K)	Injection pressure (MPa)
1	0.28	0.9	279	4
2	0.38	0.9	279	4
3	0.18	0.9	279	4
4	0.28	0.7	279	4
5	0.28	0.8	279	4
6	0.28	0.9	280	4
7	0.28	0.9	281	4
8	0.28	0.9	279	3.5
9	0.28	0.9	279	3
10	0.28	0.9	279	4
11	0.38	0.9	279	4
12	0.18	0.9	279	4
13	0.28	0.8	279	4
14	0.28	0.7	279	4
15	0.28	0.9	279	3.5
16	0.28	0.9	279	3
17	0.28	0.9	279	4

in a field-scale reservoir. Detailed validation of the previous version of the code has been reported by Khetan *et al.* [30]. In the present study, the field scale reservoir was 100 m long and initially filled with water, hydrate and methane gas at the hydrate equilibrium pressure of 15 MPa and temperature of 287 K. One end of domain was insulated and other was suddenly subjected to a depressurization pressure of 2 MPa. Owing to depressurization, the pressure inside the reservoir decreased, thus leading to the dissociation of hydrates. Simultaneously, there was a decrease in hydrate saturation and increase in gas saturation. As hydrate dissociation is an endothermic reaction, it leads to a reduction in temperature of the reservoir. The numerical scheme used in the present study captured the evolution of the total gas pressure, temperature, and other related variables within the reservoir with good accuracy. The results of the validation exercise are summarized in Figures 3a–3d.

3.2 Grid independence

Two studies related to grid size independence and time step independence were carried out. By progressively decreasing the step sizes, it were confirmed that a grid size of 2 m and time step of 0.5 s were acceptable. These values have been adopted for all subsequent calculations.

4 Results and discussion

Altogether, seventeen case studies of CO_2 injection into the reservoir are simulated by varying important parameters as given in Tables 1 and 2. Simulations are divided into the following two categories – non-isothermal injection (cases 1–9), isothermal injection (cases 10–16) and CO_2 injection in porous media partially filled with CH_4 gas and water (case 17). Case 1 is a baseline configuration that is compared with others. A total of 40 months of physical CO_2 injection is considered. The initial conditions and parameters for case 10 are similar to case 1 except for the presence of CH_4 in the reservoir instead of CO_2 at the time of injection, a study of CO_2 injection in depleted natural gas reservoir.

Results are presented below in the following sequence. Pressure, temperature, and saturation distributions for the baseline configuration (case 1) are presented in detail. The data is compared with the isothermal model (case 10). The effects of varying porosity (ϕ), initial water saturation (S_{w0}), initial reservoir temperature (T_i) and injection pressure (P_{inj}) with isothermal and non-isothermal models are systematically compared. Case study 17 involving the presence of methane in the reservoir is finally presented and compared with the baseline configuration. Thermal conductivity of a porous medium has significant effect on hydrate formation. This aspect is evaluated by comparison of isothermal and non-isothermal simulations. It should be noted that the isothermal limit is achieved with an infinite thermal conductivity wherein no change in reservoir temperature is allowed during the exothermic hydrate formation. Non-isothermal conditions emerge when thermal conductivity of the medium is prescribed as finite during the solution of the thermal energy equation for predicting spatio–temporal changes in reservoir temperature. In addition, changes in reservoir temperature depend on the reaction rate and the enthalpy of hydrate formation and dissociation.

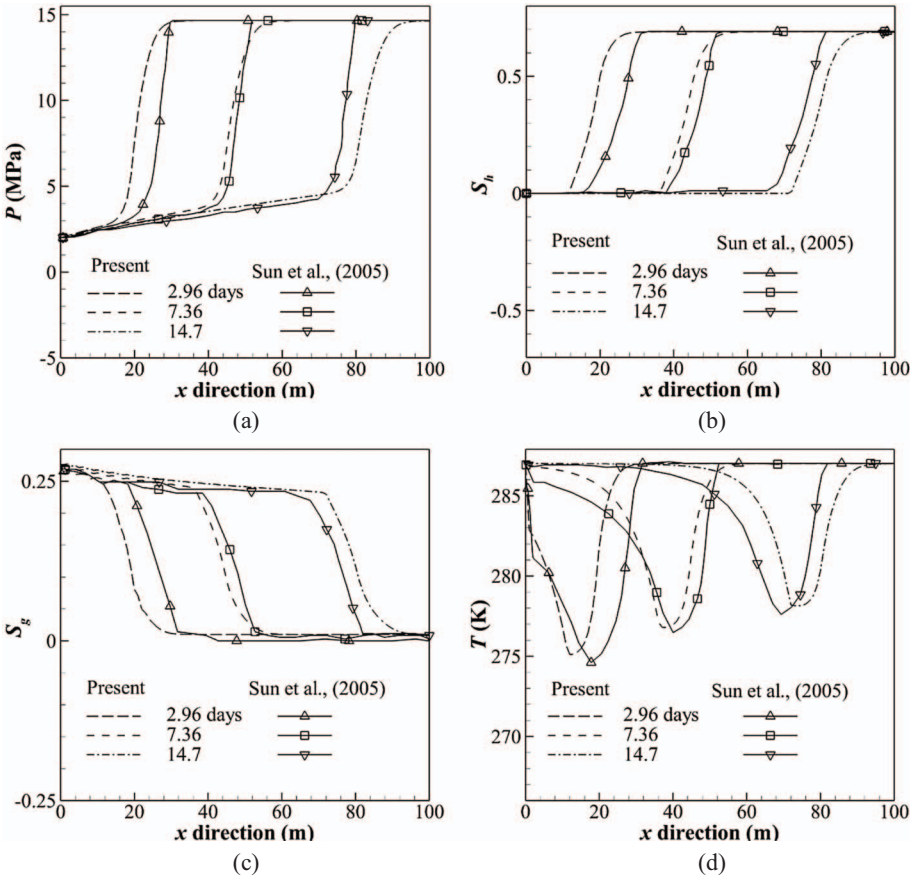

Fig. 3. Validation of numerical solver by comparison of numerical simulation of [26] with the present simulator for depressurization of a 100 m long horizontal field scale reservoir.

4.1 Non-isothermal injection (case 1)

Initially, the reservoir is at a pressure of 2.51 MPa and 279 K temperature in the baseline simulation. It is 90% saturated with water and contains no initial hydrate. CO_2 gas, at a pressure of 4 MPa and 279 K, is injected from the injection well ($x = 0$ m). Results are shown in Figures 4a–4e and 5a and 5b over the length of the reservoir for a time period of 40 months. Temporal and spatial variation of gas pressure is shown in Figure 4a while variations in hydrate, water, and gas saturations are shown in Figures 4b–4d. Temperature evolution is presented in Figure 4e. The quantities of interest such as the total injected CO_2 mass and rate of CO_2 injection are shown in Figure 5a. CO_2 mass present in hydrate and gaseous forms are individually shown in Figure 5b. As the injection starts, the pressure in the reservoir increases, causing the CO_2 to form hydrate. Pressure variation in the reservoir is governed by a diffusion-like equation. Its diffusivity is directly proportional to permeability of the media, relative permeability of gas phase and inversely proportional to gas viscosity. Higher the permeability, the faster is pressure diffusion. The present simulation shows that pressure diffuses to the end of the 500 m long reservoir over a period of nearly 20 months. Later, there is an increase in pressure up to ~2.6 MPa from the initial pressure of 2.5 MPa, and is shown in Figure 4a.

Figure 4b shows spatial distribution of hydrate saturation at the end of 2, 12, 20, and 40 months after the start of CO_2 injection. As soon as pressure in the reservoir goes above the hydrate equilibrium pressure, CO_2-hydrate formation starts. Its saturation in the reservoir increases with time but the distribution is seen to be non-uniform. The overall hydrate reaction is slow since, even after 40 months of injection, the maximum hydrate saturation in the reservoir is approximately 0.0015. This number is quite small when compared to the prevailing values of water and gas saturations. One of the difficulties that adversely affect CO_2 injection in a geological setting is the higher quantity of hydrate formation near the injection well. The blockage effect leading to reduction in porosity may result in the discontinuance of injection. In present study, hydrate saturation, after 40 months of injection is small and its adverse impact on injection may be considered insignificant.

The primary reason for higher hydrate formation near the injection well is the combination of greater gas pressure and water saturation at this location. A closer observation of Figure 4b suggests that location of highest hydrate saturation slowly shifts away from the injection well with progress of time. The maximum hydrate saturation in the

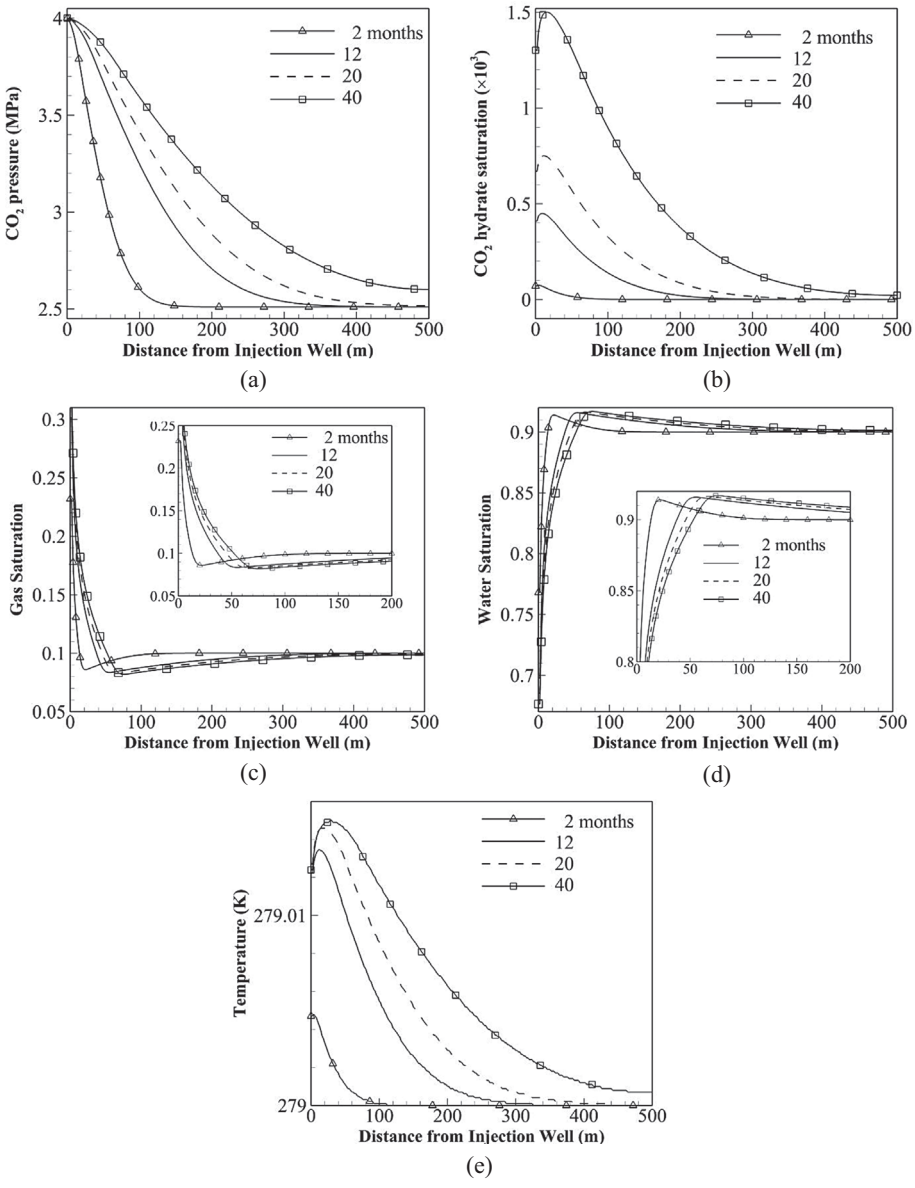

Fig. 4. Test case 1 (base case): time evolution of (a) CO_2 pressure, (b) CO_2 hydrate saturation, (c) gas saturation, (d) water saturation, and (e) temperature. Injection parameters are given in Table 1. Simulation is carried out for physical injection duration of 40 months.

reservoir after two months of injection is very close to the well but moves to a distance of 20 m away from well after 40 months. This behaviour is explained from the distribution of water saturation and gas pressure in the reservoir at various instants of time. Equation (10), the hydrate kinetic equation, suggests that the formation rate is directly proportional to the difference between existing gas pressure and equilibrium pressure at the local temperature, namely $(P_g - P_{eq})$. In addition, it depends on the hydrate formation surface area, A_{SH} and aqueous saturation, S_w. Pressure difference $P_g - P_{eq}$, is a major driving force for the reaction kinetics. Hence, as the gas pressure builds up in the reservoir, the amount of hydrate formed increases. In turn, higher hydrate saturation provides larger surface area for the hydrate reaction.

Higher water content also increases the reaction rate as it is the major fraction of a hydrate molecule. Thus, the trends in water saturation provide a good idea on the shift in location of the maximum gas hydrate saturation. Water saturation plots as given in Figure 4c, predict decreasing water content near the injection well and at the same time increasing water content, >0.9, away from well. Gas is injected at high pressure from injection well which forces resident water to move towards the interior of the reservoir. As water is not able to move faster due to the permeability constraint, a localised increment in water saturation is

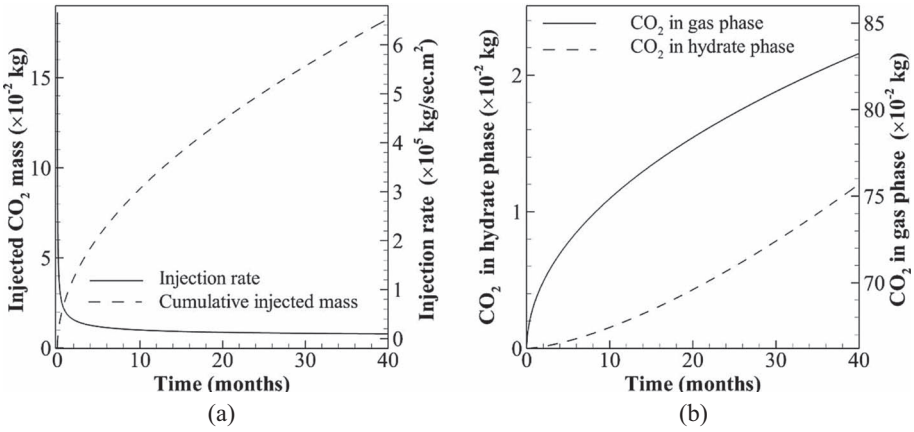

Fig. 5. Test case 1 (base case): time evolution of (a) total mass of CO_2 gas injected and injection rate for a cross sectional area of 10 m^2 and (b) accumulated mass of CO_2 in hydrate and gaseous form. Injection parameters are same as for Figure 5.

observed some distance away from well. Position of this localised high-water content slowly moves towards the other end thus gradually increasing water saturation deeper into the reservoir. Gas phase saturation, Figure 4d, has a behaviour similar to water phase but in the opposite direction. Specifically, gas saturation increases near the injection point then decreases below initial saturation before recovering the initial value. Gas saturation is below its initial value at locations where water content is higher than its initial value since there is competition between these fluids to occupy the same pore space of the reservoir. The point of maximum hydrate saturation is that location where overall conditions are favourable for kinetic reactions. In contrast, the shift in the location of maximum water content arises from applied gas pressure to the reservoir permeability constraint. As a result, the point of maximum hydrate saturation trails the maximum water saturation at any instant of time.

Figure 4e shows the temperature variation in the reservoir at time instants of 2, 12, 20, and 40 months after the start of the injection process. It is observed that with the progression of hydrate formation, temperature in the reservoir increases with time. However, the quantum of hydrate formed is small and thus the extent of temperature change is negligible, being about 0.015 °C after 40 months of injection. Similar to hydrate saturation, the peak temperature shifts away from the well with time. The speed of this shift is consistent with that observed in the hydrate saturation data. The temperature variation shown in the present study differs from previous studies such as Zatsepina and Pooladi-Darvish [24] and Abe *et al.* [20]. These authors have reported a significant rise in reservoir temperature after CO_2 injection suggesting a higher rate of hydrate formation. However, there are several differences between their work and the present study. Zatsepina and Pooladi-Darvish [24] employed instantaneous hydrate formation condition in their model whereas the present work considers rate limiting hydrate kinetics. Similarly, Abe *et al.* [20] used a much lower initial temperature in their experimental work from the equilibrium temperature which caused significantly higher hydrate formation and temperature rise. In the present work, hydrate formation starts from a gaseous state close to the equilibrium condition.

While CO_2 injection in geological reservoirs is an energy intensive process, it is necessary that energy consumption should be minimized for a given amount of CO_2 injected. Numerical simulations provide useful insight into reservoir response against the injection process. These can be utilized for devising better gas injection strategies leading to reduction of the overall cost of injection. At the same time, the injection process can be made safer and environment friendly.

The cumulative mass of injected CO_2 and injection rates are two important quantities that determine the potential of the reservoir for CO_2 sequestration. Time variation of these two quantities for the baseline non-isothermal injection arrangement is shown in Figure 5a. It is seen that the total quantity of injected gas increases over time. Since the reservoir is being pressurized, the applied pressure gradient decreases and thus the injection rate also monotonically decreases with time. The injection rate is initially in excess of 0.6 kg/s and diminishes to less than 0.05 kg/s in a period of two months. Over a period of 40 months, the injection rate is as small as 0.01 kg/s. The total injected CO_2 (kg) shows polynomial growth for the initial two months, followed by slow linear growth, being proportional to the injection rate. One of the important objectives of the present study is the evaluation of the extent of CO_2-hydrate formation and identification of parameters relevant to increasing the rate of hydrate reaction so that safe trapping of the injected CO_2 at the highest quantity can be ensured. It may be stated here that geological storage of CO_2 in hydrate form is safer than the gaseous phase, and the storage is afforded in much larger amounts. These twin objectives can be achieved only when the hydrate formation rate is simultaneously increased.

Figure 5b shows the comparison between the relative amounts of CO_2 mass in gaseous and hydrate forms and its evolution with time. It is seen that the amount of CO_2 stored in hydrate form is nearly two orders of magnitude

smaller than the CO_2 mass stored in gaseous form even after 40 months of continuous injection. At the same time, it is clear from Figure 5b that the trend of CO_2 mass stored in gaseous form flattens in time whereas in hydrate form, shows a continuous upward trend. Under favourable conditions of porosity, pressure, and temperature, a reversal in trend may be anticipated.

It emerges from analysis that quantities of interest such as hydrate saturation at the end of 40 months and change in temperature are small and hence, not significant. However, the results presented are of value because (a) CO_2 burial timescales are substantially longer and (b) practical applications will include enhancement technologies for which the baseline data of the present study is essential. The model discussed in the present study can be extended to include such enhancement methods. We have demonstrated one such generalization by including CO_2 injection in the presence of methane. Other extensions such as reservoir heterogeneity and changes in hydrological properties such as relative permeability derived from experiments can be comfortably incorporated.

The sensitivity of the CO_2 storage data, either in gaseous form or as a hydrate to the reservoir and injection parameters are discussed in the following sections.

4.2 Sensitivity to important parameters

The effect of variation of parameters such as porosity, initial water saturation, initial reservoir temperature, and injection pressure, on the total injected mass of CO_2 and formed hydrate are discussed in the present section. The choice of parameters is summarized in Table 2. Though isothermal and non-isothermal formulations are compared in the baseline simulation (Sect. 4.1), results below are discussed only with the non-isothermal model. It is expected that the two will continue to show similar trends in the predicted variables.

4.2.1 Effect of porosity

Porosity is a direct measure of void space fraction of reservoir volume. Increase in porosity results in an increase in pore volume, and hence an increase in the storage capacity. However, the responses of other field variables such as temperature, pressure, hydrate saturation to variation in porosity are not straight-forward for a reactive system. Since the quantum of hydrate formation is small, it is expected that increase in pore volume with porosity will provide additional gas storage and will be a major contributing factor.

Results are presented for 40 months of CO_2 injection into the reservoir for three different porosities, $\phi = 0.18$, 0.28, and 0.38. Figures 6a–6c show temporal evolution of pressure, hydrate saturation, and temperature after 6 and 36 months of injection. Figure 6d shows time evolution of the total injected mass for CO_2 for the three porosities.

With increase in porosity, a marginal reduction in reservoir pressure is recorded. This reduction is caused by increase in effective permeability and hence lower hydraulic resistance to gas flow as higher permeability requires a lower pressure gradient for a given flux of gas flow. Figure 6b shows the variation in CO_2 hydrate saturation for three different porosities. The extent of variation in saturation is insignificant as very marginal decrease in hydrate saturation is recorded when porosity is increased from 0.18 to 0.38. This response of the reservoir is consistent with changes seen with respect to gas pressure where a marginal decrease in the pressure for increase in porosity is observed. However, the volumetric amount of hydrate formed is higher for higher porosity as fraction of volume occupied is higher. Figure 6c shows the variation of reservoir temperature at 6 and 36 months after initiation of injection. It is seen that for higher porosity, increase in reservoir temperature is higher although hydrate saturation is marginally lower. This result arises due to higher energy released during hydrate formation for the case when porosity is higher as volumetrically higher CO_2 converts to hydrate. Another factor which contributes to increase in temperature is reduction in volumetric heat capacity of the reservoir with increase in the porosity. It is observed that for porosities 0.18 and 0.38, an increase in average reservoir temperature for the latter is nearly twice of the increase observed at the lower porosity. Figure 6d shows the comparison of injected CO_2 mass for three porosities. A higher porosity reservoir clearly stores higher CO_2 mass as it shows an approximately linear variation with porosity.

4.2.2 Effect of initial water saturation

Three values of initial water saturation, $S_{w0} = 0.7$, 0.8, and 0.9, are shown in Figures 7a–7d for the spatial evolution of gas pressure, hydrate saturation, temperature, and amount of gas injected at 6 and 36 months after initiation of gas injection. Figure 7a shows that the variation in reservoir water saturation has significant effect on gas phase migration inside the reservoir. For higher water saturation, gas pressure in the reservoir is comparatively lower except at the zone around the injection well. Near the well, pressure is slightly higher for higher saturation when compared to gas pressure at lower water saturations. This behaviour arises from a change in gas relative permeability with change in water saturation. Higher aqueous phase saturation reduces the gas phase relative permeability thus obstructing the flow of gas. Diffusion rate of gas pressure inside the reservoir is thus lowered when compared to a reservoir with lower initial water saturation. A reduction in gas phase relative permeability increases pressure in the zone around the well because of obstruction to gas flow as seen in Figure 7a. As the relative permeability, k_{rg}, is a non-linear function of water saturation, changes in pressure will not linearly scale with water saturation. Specifically, a higher reduction in initial saturation will yield a higher increase in gas pressure.

Figure 7b shows the temporal evolution of hydrate saturation for three initial water saturations at 6 and 36 months after gas injection. Relative to the baseline simulation ($S_{w0} = 0.9$), a peak in hydrate saturation near the injection well is observed for lower saturations ($S_{w0} = 0.7$ and 0.8) as well. This peak is higher for higher initial water content and is realized at both 6 and 36 months.

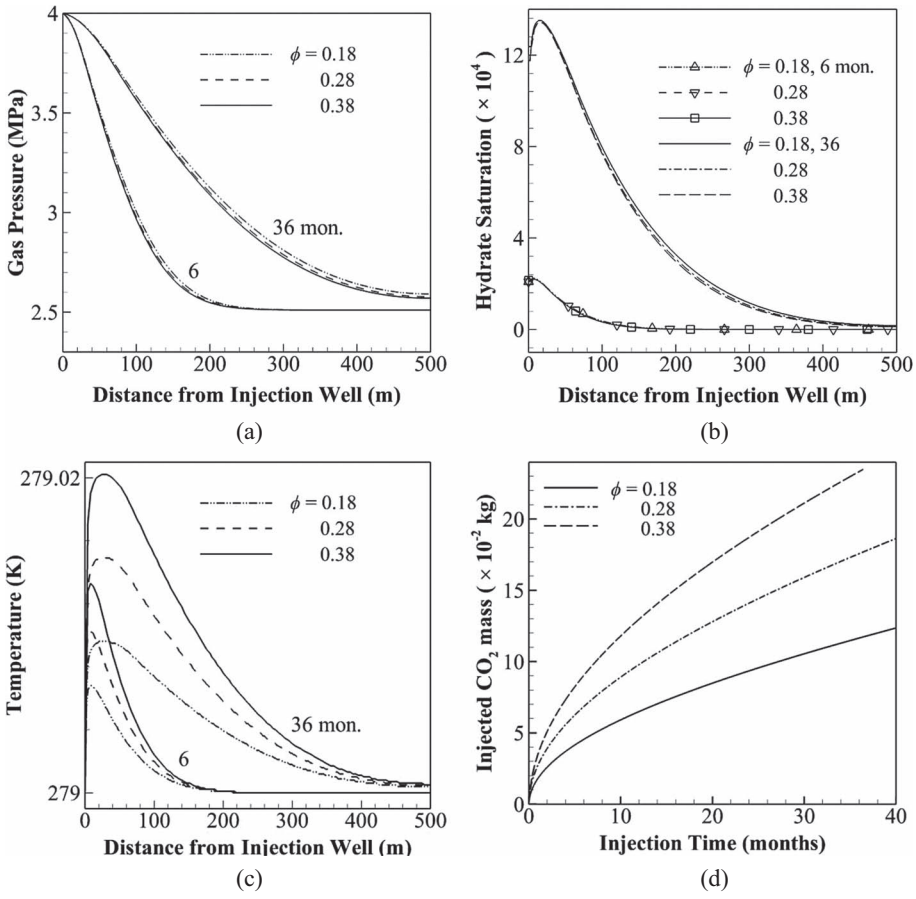

Fig. 6. Time evolution of (a) gas pressure, (b) hydrate saturation, (c) temperature distributions after 6 and 36 months of injection, and (d) mass of CO_2 injected for three different reservoir porosities. Injection parameters are same as given in Table 1 except for porosity. (Test cases 1–3).

A reduction in the hydrate saturation from the peak value is observed in the three initial water saturations but the extent of reduction is greater when the initial water content is high. From the hydrate saturation graphs, it may be concluded that the hydrate saturation is nearly equal for the three initial water saturations, though lower initial water content allows for more uniform hydrate formation as seen in Figure 7b. Specifically, lower initial water content allows higher gas pressure in the interior of the reservoir and assists in higher hydrate formation. For the same reason, peak hydrate saturation is lower for low water content. Hence, the combined effect is a more uniform hydrate distribution for low initial water saturation as compared to other two values studied.

Temperature distribution in the reservoir for the three values of initial water saturations is given in Figure 7c at time instants of 6 and 36 months. Temperature distribution shows a trend that are very similar to, and consistent with, hydrate saturation. Correspondingly, a lower peak temperature for low initial water content and higher temperature rise in the interior are obtained. It is interesting to note that these plots divide the reservoir in two zones – for a given S_{w0}, a zone closer to the well shows higher hydrate formation activity for high initial water content and hence a higher temperature rise; a second zone away from the well sees lower hydrate formation activity and a smaller increase in temperature.

Figure 7d shows the temporal evolution of accumulated CO_2 mass in the reservoir for three different values of initial water saturation. It is clear from these data that a lower initial quantum of water allows more CO_2 to be accumulated and at the same time, supports uniform hydrate formation, as also seen in Figure 7b. Low initial water content further reduces the chances of well blockage due to comparatively lower hydrate formed near the injection well. Higher injection is possible due to higher gas phase relative permeability for lower water content. It allows for quicker increase in gas pressure of the reservoir resulting in hydrate reactions with greater spatial uniformity. At the same time, lower water content allows more space for the gaseous phase, thus allowing more gas to be accumulated.

From the above analysis, it is concluded that optimal water content in the reservoir is possible that augments

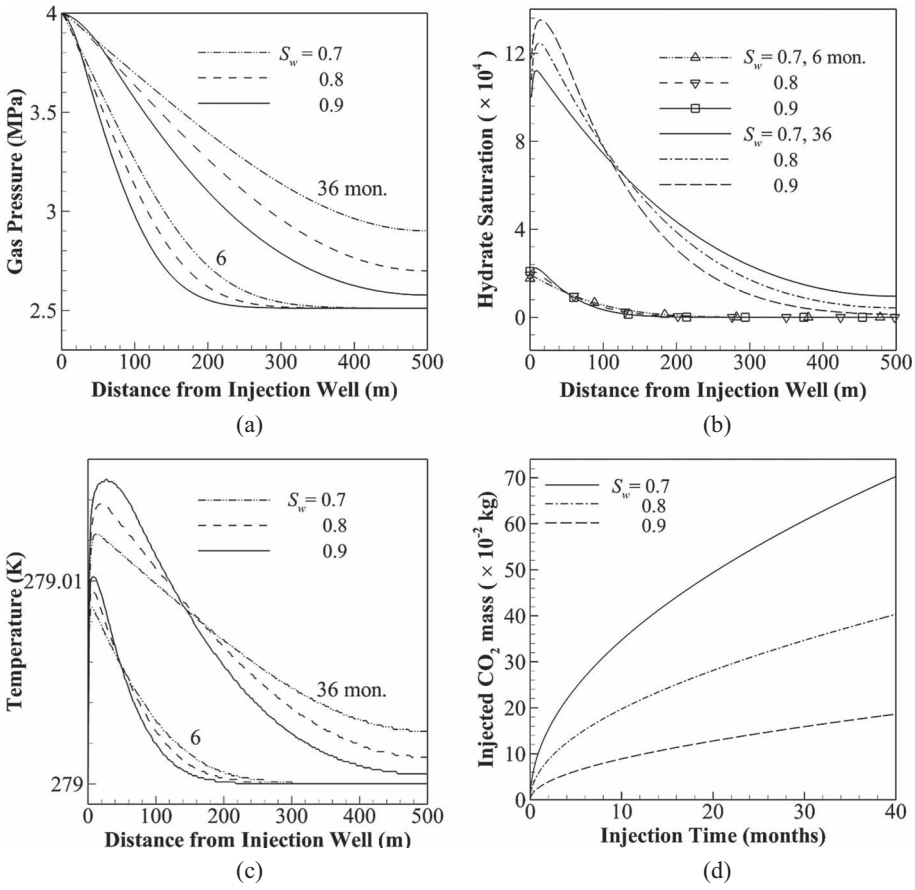

Fig. 7. Time evolution of (a) gas pressure, (b) hydrate saturation, (c) temperature distributions at 6 and 36 months after initiation of CO_2 injection, and (d) total mass of CO_2 gas injected after 40 months of injection for three different values of initial water saturation (S_{w0}) in porous layer. Injection parameters are same as given in Table 1 except S_{w0}. (Test cases 5–7).

hydrate formation and at the same time permits more CO_2 to be structurally trapped within.

4.2.3 Effect of initial reservoir temperature

Figures 8a, 8b, and 8d show results for temporal evolution of gas pressure, hydrate saturation and total injected CO_2 mass for three values of initial reservoir-temperatures, 279 K, 280 K, and 281 K. The initial reservoir pressure is kept identical in the three simulations, being equal to 2.51 MPa. From Figure 8a, it is clear that reservoir pressure is not affected much due to variation of 1–2 K in reservoir temperature. Only a slight variation in pressure is observed after 36 months of injection with a higher temperature reservoir having a slightly higher pressure. The difference in hydrate formation activity is affected significantly by changes in reservoir temperature as shown in Figure 8b. In this figure, variation in hydrate saturation after 6 and 36 months of CO_2 injection is shown. Peak value of CO_2 hydrate saturation is reduced by almost 50% if the temperature of the reservoir is increased by 2 K. Further, high reservoir temperature adversely affects the kinetics of hydrate formation. The reason for reduced formation rate is increased P_{eq} for higher temperature thus lowering the reaction kinetics. The effect of initial reservoir temperature is shown by Figure 8c wherein the difference between injection pressure and CO_2 hydrate phase equilibrium pressure ($P_{inj} - P_{eq}$) for three initial reservoir temperatures is indicated. It is clear from the graph that lower initial reservoir temperature has higher $P_{inj} - P_{eq}$, confirming increased formation rate. As temperature of the reservoir increases, the driving pressure difference $P_{inj} - P_{eq}$ decreases, causing retardation in the formation kinetics. It is to be recorded that the sequestered CO_2 hydrate decreases by 72% for a temperature increase from 279 K to 280 K. Cumulative injected mass of CO_2 as shown in Figure 8d suggests a marginal reduction in time.

4.2.4 Effect of injection pressure

Simulations at three injection pressures of 3, 3.5, and 4 MPa are carried out and the spatio-temporal distribution of the quantities of interest is shown in Figures 9a–9d. Variables under study are gas pressure, hydrate saturation, temperature and the quantum of the injected CO_2 mass. Evaluation of injection pressures lower than the one considered in the

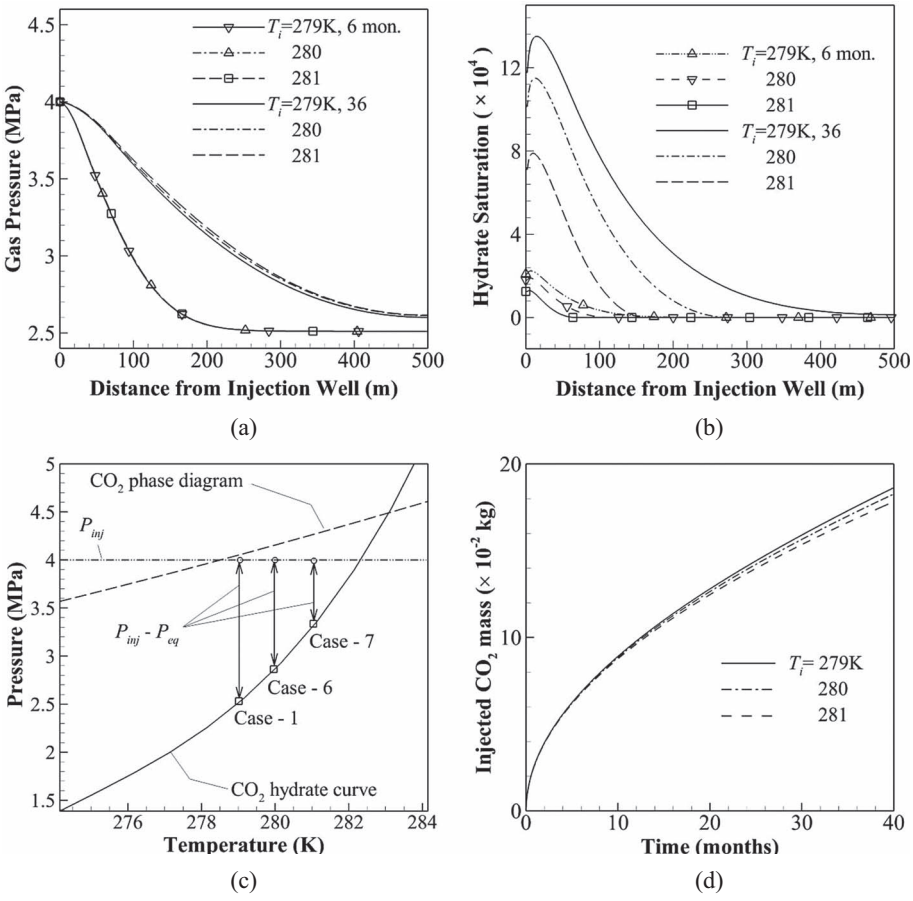

Fig. 8. Test cases 1, 6, and 7: non-isothermal model: time evolution of (a) gas pressure, (b) hydrate saturation at 6 and 36 months of CO_2 injection, (c) schematic showing the difference between P_{inj} and P_{eq}, and (d) total mass of CO_2 gas injected after 40 months of injection for three different values of initial reservoir temperature (T_i) in porous layer. Injection parameters are same as given in Table 1 except T_i.

baseline configuration (<4 MPa) alone is chosen because any further increase in injection pressure will lead to the formation of liquid CO_2. The model described in Section 3 can accommodate up to two mobile phases (gas and water) but not the possibility of liquid CO_2.

Figure 9a shows the spatial variation in gas pressure inside the reservoir for three injection pressures at time instants of 6 and 36 months after initiation of injection. Qualitatively, the three data sets are similar but pressure build-up is faster for higher injection pressure. This is because of a larger pressure gradient at the injection well set up for similar reservoir parameters. Figure 9b shows the spatial distribution of hydrate saturation for the three injection pressures. It is evident that higher injection pressure results in higher hydrate saturation. It is also evident that reduction in hydrate saturation is sharper with each decrement in pressure. Specifically, the difference in peak hydrate saturation values between injection pressures of 4 and 3.5 MPa is smaller as compared to the difference between 3.5 and 3 MPa. Figure 9c shows temperature variation for the three test cases under consideration. It is clear from the data that a higher peak temperature in the reservoir is recorded for higher injection pressure, consistent with the fact that higher hydrate formation activity releases a greater amount of thermal energy. Figure 9d shows the temporal evolution of injected CO_2 mass for the three injection pressure. It is evident that an increase in pressure results in an increase in injected mass of CO_2 stored both in hydrate and gaseous forms. When the pressure is reduced from 4 MPa to 3 MPa, a 70% reduction in hydrate saturation is observed. At the same time the cumulative injected CO_2 mass reduces by a factor greater than 3.5.

4.2.5 Injection in depleted reservoir

Results for CO_2 injection in a depleted hydrate reservoir is shown in Figures 10a–10e for parameters similar to the baseline configuration except that CH_4 gas is initially present in the reservoir instead of CO_2. In a depleted hydrate reservoir, a combination of natural gases is present but for model simplicity, it is assumed that the reservoir contains only gaseous methane. Figure 10a shows the variation in total pressure in the reservoir at 2, 12, 20, and 40 months

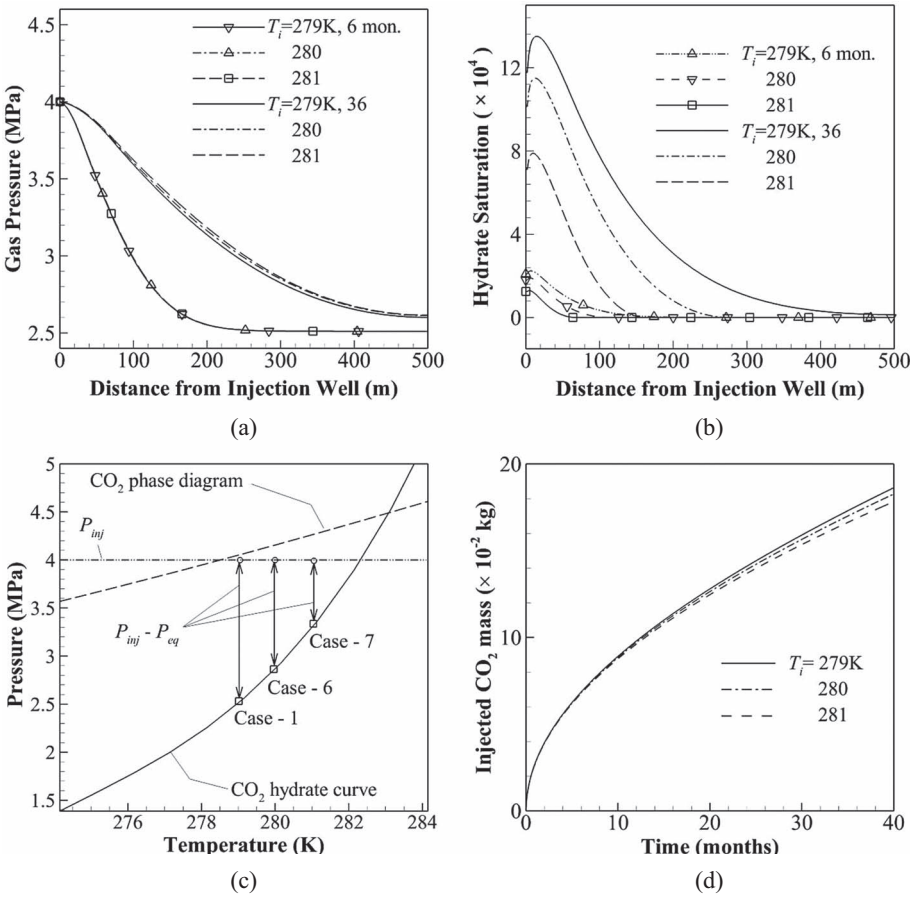

Fig. 9. Test cases 1, 8, and 9: non-isothermal model: time evolution of (a) gas pressure, (b) hydrate saturation, (c) temperature distributions at 6 and 36 months of CO_2 injection, and (d) total mass of CO_2 gas injected after 40 months of injection for three different values of injection pressure (P_{inj}) in porous layer. Injection parameters are same as given in Table 1 except P_{inj}.

after start of the injection process. When compared to the baseline configuration (Sect. 4.1), pressure is seen to be slightly lower. It is seen that average reservoir pressure changes from 3.102 MPa to 3.038 MPa, a marginal decrease. This is due to a higher increase in reservoir temperature seen in the baseline study as compared to the present simulation that shows negligible temperature rise. The increase in temperature is related to increased CO_2 hydrates formation due to the presence of only CO_2 gas in the reservoir. Figure 10b shows the distribution of CO_2 gas partial pressure. When injected at higher pressure from the well, CO_2 enters the reservoir due to the combined effect of diffusion as well as advection. It is evident that increase in CO_2 partial pressure is slow since at the end of 40 months of injection, its presence is felt up to a distance less than 100 m from the well. In contrast, total pressure has steadily risen in the entire reservoir. Saturation data of the gas phase and water are presented in Figures 10c and 10d. There is no visible difference with the baseline configuration. Temporal variation for CO_2 hydrate saturation is given in Figure 10e. It is seen once again that CO_2 hydrate formation is very small when compared to a reservoir initially filled with CO_2 gas. At the same time CO_2 hydrate formation is restricted to a short distance of 10 m, from the injection well. Comparative estimate of CO_2 hydrate formation shows one order of magnitude decline. There, it is noteworthy that CH_4 hydrate formation will not take place for the present set of parameters since injection pressure is small and falls outside the regime of stable CH_4 hydrate.

4.2.6 Isothermal and non-isothermal comparison

Two separate studies carried out with isothermal and non-isothermal frameworks have been compared. It is found that the temporal and spatial evolution of important field variables as shown in previous subsections is similar. Hence, the results for isothermal simulation are not shown here. It is postulated that with very slow hydrate formation kinetics, the effect of small variations in reservoir temperature will only marginally affect the injected CO_2 mass and formed hydrate.

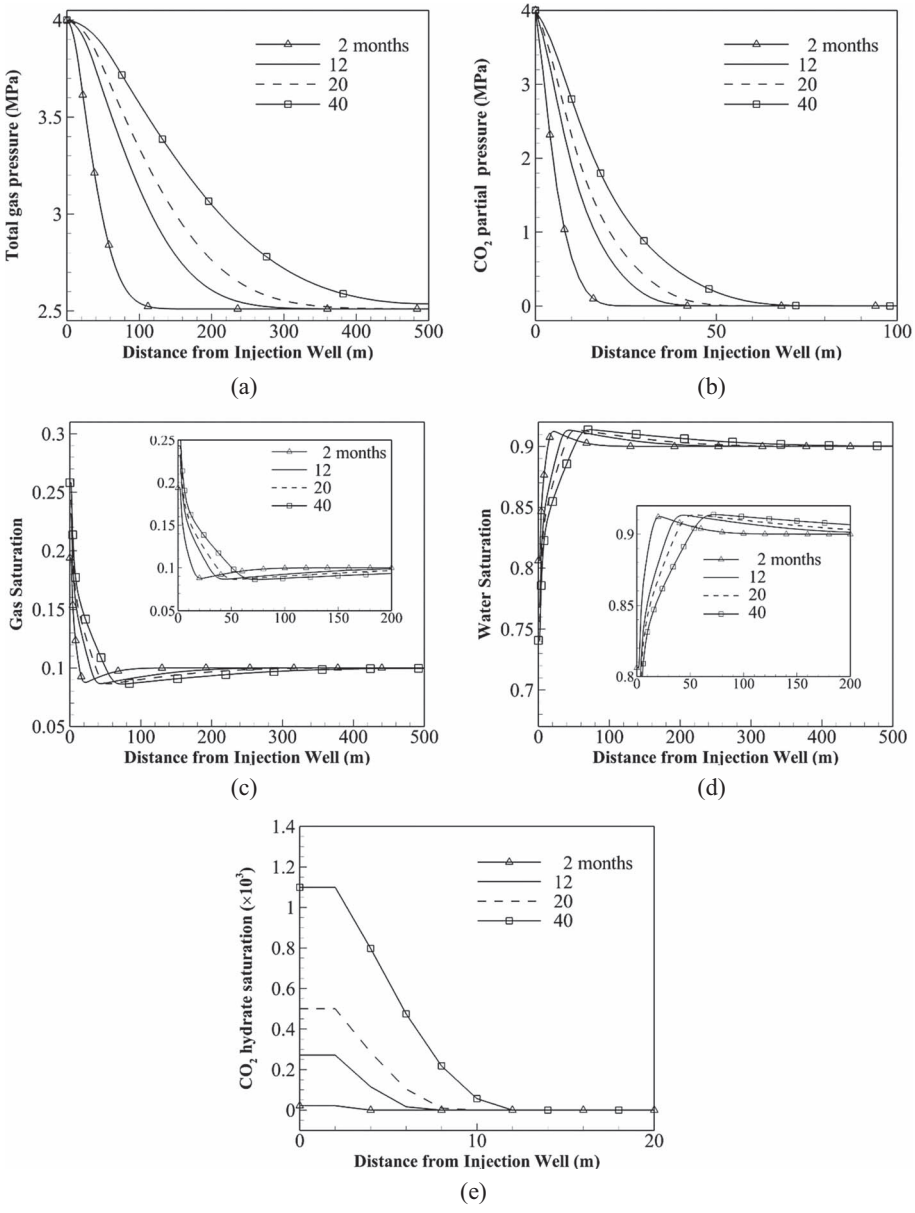

Fig. 10. Test case 17, non-isothermal model: time evolution of (a) total gas pressure, (b) CO_2 partial pressure, (c) gas saturation, (d) water saturation, and (e) CO_2 hydrate saturation at 2, 12, 20, and 40 months after start of injection process. Parameters are as given in Table 1 except initial mole fractions of CO_2 and CH_4 gases which are, $x_{c0} = 0$ and $x_{m0} = 1$ respectively.

5 Conclusion

A numerical study of CO_2 sequestration as hydrate in a thermodynamically suitable reservoir is reported in this study. Quantities of interest include injected CO_2 mass and the portion of it forming hydrate with the water content within the reservoir. Simulations are classified as isothermal and non-isothermal. Comparative studies are carried out to address the effect of porosity, injection pressure, initial water saturation, and reservoir temperature. Overall, simulations show that the hydrate reaction kinetics is slow and the fraction of gas stored as hydrate is small. However, it progressively increases with time. Since the heat release due to chemical reactions is small, the isothermal and non-isothermal models yield practically identical outcome. Specific conclusions drawn in the present work are given below:

1. Injected CO_2 mass linearly increases with increasing porosity though gas pressure and hydrate saturation show marginal deviation. Amount of CO_2 sequestered as hydrate increases with increasing porosity as volume of the hydrate formed goes up.
2. Initial reservoir water saturation is an influential parameter as far as CO_2 mass storage is concerned. Higher initial water content adversely affects gas

phase permeability and thus gas inflow. As water saturation decreases from 0.9 to 0.7, injected CO_2 mass increases by a factor of 3.5. Moreover, the distribution of hydrate formation in the reservoir becomes more uniform with decreasing water saturation.

3. Initial reservoir temperature shows a significant influence on the stored CO_2 hydrate. A 72% reduction in hydrate is attained for a temperature increase from 279 K to 281 K.
4. Injected mass of CO_2 varies significantly with injection pressure. It decreases by a factor of 3.5 and the CO_2-hydrate formed reduces by 70% for a reduction in injection pressure from 4 MPa to 3 MPa.
5. Higher hydrate formation and temperature variation is seen near the injection well. The hydrate formation rate within 200 m from the injection well is one order of magnitude higher than the interior.
6. An order of magnitude reduction in average CO_2 hydrate sequestered in a methane-filled reservoir is realized when compared to an initially CO_2 filled reservoir.

It is to be noted that the present work differs from previous simulation and experimental studies on CO_2 sequestration in parametric terms. These include the phase of the injected gas and a lower initial reservoir temperature. In terms of modeling, instantaneous hydrate formation kinetics is assumed in the literature, unlike the finite-time reaction chemistry considered in the present work. For these reported conditions, hydrate formation is faster that what has been reported in the present work. It is suggested that experiments similar to [20] with the parameters of the present work be carried out for a direct validation of the model predictions.

References

1 Leung D.Y.C., Caramanna G., Maroto-Valer M.M. (2014) An overview of current status of carbon dioxide capture and storage technologies, *Renew. Sustain. Energy Rev.* **39**, 426–443.

2 Vedachalam N., Srinivasalu S., Rajendran G., Ramadass G.A., Atmanand M.A. (2015) Review of unconventional hydrocarbon resources in major energy consuming countries and efforts in realizing natural gas hydrates as a future source of energy, *J. Nat. Gas Sci. Eng.* **26**, 163–175.

3 Celia M.A., Nordbotten J.M. (2009) Practical modeling approaches for geological storage of carbon dioxide, *Groundwater* **47**, 5, 627–638.

4 Myer L. (2011) *Global Status of Geologic CO_2 Storage Technology Development*, United States Carbon Sequestration Counc. Rep. July, Vol. **2011**.

5 Doughty C., Freifeld B.M., Trautz R.C. (2008) Site characterization for CO_2 geologic storage and vice versa: The Frio brine pilot, Texas, USA as a case study, *Environ. Geol.* **54**, 8, 1635–1656.

6 Shindo Y., Fujioka Y., Ozaki M. (1993) New concept of deep sea CO_2 sequestration, in: *Proc. Int. Symp. on CO_2 Fixation & Efficient Utilization of Energy*, pp. 307–314.

7 Fujioka Y., Ozaki M., Takeuchi K., Shindo Y., Yanagisawa Y., Komiyama H. (1995) Ocean CO_2 Sequestration at the Depths larger than 3700 m, *Energy Convers. Manag.* **36**, 6, 551–554.

8 Koide H., Shindo Y., Tazaki Y., Iijima M., Ito K., Kimura N., Omata K. (1997) Deep sub-seabed disposal of CO_2 – The most protective storage –, *Energy Convers. Manag.* **38**, S253–S258.

9 Jenkins C.R., Cook P.J., Ennis-King J., Undershultz J., Boreham C., Dance T., de Patrice C., Etheridge D.M., Freifeld B.M., Hortle A. (2012) Safe storage and effective monitoring of CO_2 in depleted gas fields, *Proc. Natl. Acad. Sci.* **109**, 2, E35–E41.

10 Cote M.M., Wright J.F., Dallimore S.R. (2008) Overview of regional opportunities for geological sequestration of CO_2 as gas hydrate in Canada, in: *6th International Conference on Gas Hydrates, July 6–10, Vancouver, British Columbia, Canada*.

11 Cote M., Wright F. (2010) Geological potential for sequestration of CO_2 as gas hydrate in the Alberta portion of the Western Canada Sedimentary Basin, in: *Canadian Unconventional Resources and International Petroleum Conference, 19–21 October, Calgary, Alberta, Canada*.

12 Shaw J., Brennan-Alpert P. (2004) *Technical evaluation & feasibility study on subterranean disposal of CO_2 as hydrate*, Geological Survey of Canada.

13 Sloan E.D. Jr., Koh C. (2007) *Clathrate hydrates of natural gases*, CRC Press, USA.

14 Kvenvolden K.A. (1998) A primer on the geological occurrence of gas hydrate, *Geol. Soc. Lond. Spec. Publ.* **137**, 1, 9–30.

15 Ohmura R., Mori Y.H. (1998) Critical conditions for CO_2 hydrate films to rest on submarine CO_2 pond surfaces: A mechanistic study, *Environ. Sci. Technol.* **32**, 8, 1120–1127.

16 Uchida T., Takagi A., Hirano T., Narita H., Kawabata J., Hondoh T., Mae S. (1996) Measurements on guest-host molecular density ratio of CO_2 and CH_4 hydrates by Raman spectroscopy, in: *Proceedings of the 2nd International Conference on Natural Gas Hydrates, June 2–6, 1996, Toulouse, France*, pp. 335–339.

17 Koide H., Takahashi M., Shindo Y., Tazaki Y., Iijima M., Ito K., Kimura N., Omata K. (1997) Hydrate formation in sediments in the sub-seabed disposal of CO_2, *Energy* **22**, 2–3, 279–283.

18 Qanbari F., Pooladi-Darvish M., Tabatabaie S.H., Gerami S. (2012) CO_2 disposal as hydrate in ocean sediments, *J. Nat. Gas Sci. Eng.* **8**, 139–149.

19 Qanbari F., Pooladi-Darvish M., Tabatabaie S.H., Gerami S. (2011) Storage of CO_2 as hydrate beneath the ocean floor, *Energy Procedia* **4**, 3997–4004.

20 Abe Y., Takagi Y., Kaneko A., Yamane K. (2013) Hydrodynamics of liquid CO_2 with hydrate formation in packed bed, *Int. J. Heat Mass Transf.* **65**, 95–101.

21 Zhou S., Yan H., Su D., Navaneethakannan S., Chi Y. (2018) Investigation on the kinetics of carbon dioxide hydrate formation using flow loop testing, *J. Nat. Gas Sci. Eng.* **49**, 385–392.

22 Liu Y., Wang P., Yang M., Zhao Y., Zhao J., Song Y. (2018) CO_2 sequestration in depleted methane hydrate sandy reservoirs, *J. Nat. Gas Sci. Eng.* **49**, 428–434.

23 Zhang D., Fan C., Kuang D. (2019) Impact assessment of interlayers on geological storage of carbon dioxide in Songliao Basin, *Oil Gas Sci. Technol. - Rev. IFP Energies nouvelles* **74**, 85.

24 Zatsepina O.Y., Pooladi-Darvish M. (2011) CO_2-hydrate formation in depleted gas reservoirs – A methodology for CO_2 storage, *Energy Procedia* **4**, 3949–3956.

25 Schoderbek D., Farrell H., Howard J., Raterman K., Silpngarmlert S., Martin K., Smith B., Klein P. (2013) *ConocoPhillips gas hydrate production test*, ConocoPhillips Co., Houston, TX, USA.
26 Sun X., Nanchary N., Mohanty K.K. (2005) 1-D modeling of hydrate depressurization in porous media, *Transp. Porous Media* **58**, 3, 315–338.
27 Sun X., Mohanty K.K. (2006) Kinetic simulation of methane hydrate formation and dissociation in porous media, *Chem. Eng. Sci.* **61**, 3476–3495.
28 Oldenburg C.M. (2007) Joule-Thomson cooling due to CO_2 injection into natural gas reservoirs, *Energy Convers. Manag.* **48**, 6, 1808–1815.
29 Mathias S.A., Gluyas J.G., Oldenburg C.M., Tsang C.F. (2010) Analytical solution for Joule-Thomson cooling during CO_2 geo-sequestration in depleted oil and gas reservoirs, *Int. J. Greenh. Gas Control* **4**, 5, 806–810.
30 Khetan A., Das M.K., Muralidhar K. (2013) Analysis of methane production from a porous reservoir via simultaneous depressurization and CO_2 sequestration, *Spec. Top. Rev. Porous Media* **4**, 3, 237–252.
31 Kim H.C., Bishnoi P.R., Heidemann R.A., Rizvi S.S.H. (1987) Kinetics of methane hydrate decomposition, *Chem. Eng. Sci.* **42**, 7, 1645–1653.
32 Adisasmito S., Frank R.J., Sloan E.D.J. (1991) Hydrates of carbon-dioxide and methane mixtures, *J. Chem. Eng. Data* **36**, 1, 68–71.
33 Span R., Wagner W. (1996) A new equation of state for carbon dioxide covering the fluid region from the triple-point temperature to 1100 K at pressures up to 800 MPa, *J. Phys. Chem. Ref. Data* **25**, 6, 1509–1596.
34 Muller N., Qi R., Mackie E., Pruess K., Blunt M.J. (2009) CO_2 injection impairment due to halite precipitation, *Energy Procedia* **1**, 1, 3507–3514.
35 Anderson G.K. (2003) Enthalpy of dissociation and hydration number of carbon dioxide hydrate from the Clapeyron equation, *J. Chem. Thermodyn.* **35**, 7, 1171–1183.
36 Uddin M., Coombe D., Wright F. (2008) Modeling of CO_2-hydrate formation in geological reservoirs by injection of CO_2 gas, *J. Energy Resour. Technol.* **130**, 3, 32502.
37 Uddin M., Coombe D., Law D., Gunter B. (2008) Numerical studies of gas hydrate formation and decomposition in a geological reservoir, *J. Energy Resour. Technol.* **130**, 3, 032501–032514.
38 Yousif M.H., Abass H.H., Selim M.S., Sloan E.D. (1991) Experimental and theoretical investigation of methane-gas-hydrate dissociation in porous media, *SPE Reserv. Eng.* **6**, 1, 69–76.
39 Zhao J., Shi D., Zhao Y. (2012) Mathematical model and simulation of gas hydrate reservoir decomposition by depressurization, *Oil Gas Sci. Technol. - Rev. IFP Energies nouvelles* **67**, 3, 379–385.